SYSTEMATIC EVALUATION OF BENCHMARK G4 PROBES AND G4 CLINICAL DRUGS USING THREE BIOPHYSICAL METHODS: A GUIDELINE TO EVALUATE RAPIDLY G4-BINDING AFFINITY.

E. Laigre,[1,2‡] H. Bonnet,[3‡] C. Beauvineau,[1,2] T. Lavergne,[3] D. Verga,[1,2] E. Defrancq,[3] J. Dejeu,*[3,4] M.-P. Teulade-Fichou*[1,2]

Author Affiliations

* Corresponding authors

‡ These authors have contributed equally.

[1] CNRS UMR9187, INSERM U1196, Institut Curie, PSL Research University, F-91405 Orsay, France

[2] CNRS UMR9187, INSERM U1196, Université Paris-Saclay, F-91405 Orsay, France

E-mail: mp.teulade-fichou@curie.fr

[3] DCM, UMR 5250, Univ. Grenoble Alpes, CNRS, 570 Rue de la Chimie, 38000 Grenoble, France.

[4] SUPMICROTECH, Université Franche-Comté, CNRS, Institut FEMTO-ST, 25000 Besançon, France

E-mail: jerome.dejeu@femto-st.fr

Key-words: G-quadruplex ligands, G4-binding affinity, FRET-melting, G4-FID, SPR

Abstract:

G-quadruplex DNA structures (G4) are proven to interfere with most genetic and epigenetic processes. Small molecules binding these structures (G4 ligands) are invaluable tools to probe G4-biology and address G4-druggability in various diseases (cancer, viral infections). However, the large number of reported G4 ligands (> 1000) could lead to confusion while selecting one for a given application. Herein we conducted a systematic affinity ranking of 11 popular G4 ligands vs 5 classical G4 sequences using FRET-melting, G4-FID assays and SPR. Interestingly SPR data globally align with the rankings obtained from the two semi-quantitative assays despite discrepancies due to limits and characteristics of each assay. In the whole, PhenDC3 emerges as the most potent binder irrespective of the G4 sequence. Immediately below PDS, PDC-360A, BRACO19, TMPyP4 and RHPS4 feature strong to medium binding again with poor G4 topology discrimination. More strikingly, the G4 drugs Quarfloxin, CX5461 and c-PDS exhibit weak affinity with all G4s studied. Finally, NMM and Cu-ttpy showed heterogeneous behaviors due, in part, to their physicochemical particularities poorly compatible with screening conditions. The remarkable properties of PhenDC3 led us to propose its use for benchmarking FRET-melting and G4-FID assays for rapid G4-affinity evaluation of newly developed ligands.

Introduction

Genomic DNA has the capacity to form alternative structures to the canonical double helix which are called non-B DNAs (in opposition to the B-form of the antiparallel right handed double helix). It is now well-documented that non-B DNA may strongly impact genetic and epigenetic processes.[1-3] Amongst these, G-quadruplexes (G4s) have attracted tremendous attention over the past decades.[4-6] G4s are tetrahelix structures arising in G-rich domains genome-wide and resulting from self-assembly of guanines into quartets that are further closely packed by π-stacking interactions and coordination with K^+ or Na^+ ions. G4s are currently acknowledged as potential regulators of the three canonical steps of genetic information transfer (replication, transcription, and translation) but also of numerous related processes such as DNA repair/recombination, methylome molding/epigenetic marks repositioning, RNA trafficking/stress granules formation, alternative splicing, ribosomal frameshifting and ribosomal protein production, viral genome integration, etc.[7-13] Nonetheless many questions are still open about distribution, lifetime and dynamics of DNA and RNA G4 in cells. On the structural viewpoint, G4 structures feature hydrophobic surfaces and pockets (external G-quartets, grooves) making them "easy" targets for small synthetic compounds. This has stimulated the important development of diverse chemical platforms called G4 ligands in the aim of performing specific G4 targeting. Therefore, G4 ligands are invaluable tools necessary to probe and help interrogating G4 existence and biological relevance. They have been used in multiple studies in combination with genetic approaches and cellular immunostaining strategies.[6-7, 14] Indeed small molecules binding G4s are able to recognize a large panel of G4 forming sequences as shown by microarrays studies[15] and more recently it was found that the most potent ones can even compete with G4 specific antibodies (*e.g.* BG4).[16] Since G4 ligands stabilize G4s but also promote their formation thus increasing their lifetime, some have been shown to mimic cellular phenotypes (i.e. phenocopy) such as deletion of helicases which render G4s persistent in cells.[17-19] Besides helicases, G4 ligands can also disrupt G4 interactions with other protein partners such as Nucleolin or transcription factors[20] to name a few, thereby contributing to modulate G4-mediated downstream pathways.[21-23] Finally, a number of functionalized G4 ligands have been used in chemical-sequencing approaches to capture and map G4 genome- and transcriptome-wide.[24-27] Hence G4 ligand-based approaches proved to be highly complementary to bioinformatics predictions, G4-seq and NGS analyses.[11, 28] Besides their application as mechanistic tools (probes), G4 ligands have been extensively investigated for their capacity to act as pharmacological drugs. The research efforts have mainly focused on the field of anticancer and antiviral drug discovery on the basis of clear links established between G4s and cancer biology on one hand[13, 29-30] and RNA biology and virus development on the other hand.[12, 31-33]

This is why a plethora (> 1000) of G4 ligands have been reported so far as illustrated by the number of reviews on G4 ligands that exceeds 20-50 over the past 5 years.[29, 34-36] However, these compounds feature a large range of performances both in terms of G4-binding affinity and selectivity, whereas only a few have been rigorously validated in functional assays and in cellular contexts.[9, 16, 36-39] . Consequently, the question arises as whether all the G4 ligands are equivalent in terms of G4-binding properties, for this is often stated in biological studies. In particular in the case of cellular assays the choice of an efficient G4 probe or G4 drug is of paramount importance since the pharmacological parameters (*e.g.* solubility/logP, membrane permeability, subcellular distribution) may strongly impact compound behavior.

Different experimental methods are used to characterized G4/G4 ligand interactions. They are classified in: structure-based methods, such as circular dichroism (CD), nuclear magnetic resonance (NMR) spectroscopy, and X-ray crystallography, affinity and apparent affinity-based methods, such as surface plasmon resonance (SPR), isothermal titration calorimetry (ITC), and mass spectrometry (MS), and the

fast and cheap semi-quantitative assays, the most popular being the FRET-melting and the G4-FID.[40-46] The FRET-melting assay measures the variation in melting temperature ($T_{1/2}$) of a dual fluorescently-labeled G4-forming sequence ($\Delta T_{1/2}$/°C) upon ligand binding. The G4-FID assay measures the capacity of a G4 ligand to displace the fluorescent marker Thiazole Orange (TO) bound to the G4 structure. This ability can be expressed either by DC_{50} (ligand concentration required to decrease TO fluorescence of 50%, expressed in μM) or by the percentage of TO displacement (TOD in %) measured at 1 μM ligand concentration mostly used when the complete displacement of TO is not reached (no plateau). Although $\Delta T_{1/2}$ and DC_{50} (or TOD) reflect the binding strength of the ligand/G4 interaction, their values remain intrinsically relative and are highly dependent on both internal and external parameters: $\Delta T_{1/2}$ is relative to the $T_{1/2}$ of used G4 oligonucleotide, DC_{50} (or TOD) is related to the G4-affinity of TO and both are strongly influenced by experimental conditions (ionic force, K^+ concentration, concentration of partners). Although $\Delta T_{1/2}$ and DC_{50}/TOD are perfectly fitted for rapid evaluation of binding strength and affinity ranking within a ligand series, it is difficult to correlate the values of these indicators with an affinity constant (K_D). This is especially true for $\Delta T_{1/2}$ that reflects G4-ligand affinity but is influenced by a number of parameters (number of binding sites, cooperativity between them, binding to the unfolded form).[47] As well DC_{50}/TOD are extracted from titration curves which are often difficult to be fitted for binding constant determination especially when generated from high-throughput screening (no plateau, allosteric binding sites, strong dependence on probe binding mode).[41] However, on the practical viewpoint, since both assays have been implemented at low G4 concentration (0.2-0.25 μM), a ligand showing significant effect at a moderate excess (*e.g.* 1< ligand /DNA ratio < 10) can be considered a "high affinity binder" *i.e.* with a rough estimation of apparent K_D below the μM range.[48] Additionally, using a reference compound with a known K_D for benchmarking FRET-melting and G4-FID may allow estimation of the order of magnitude of ligand G4-affinity. Nonetheless altogether these characteristics and limits make the comparison between G4 ligands and various studies difficult unless the same conditions are rigorously applied (salts and buffer concentration, G4 sequence, G4/ligand ratio, reference ligand). On the other hand, K_D values have been determined for a number of G4 ligands most often using SPR or ITC; however, this has been done mostly for single cases (NMM, RHPS4, PhenDC3, BRACO19)[49-52] and studies based on a systematic comparative approach are still rare.[53-54] Finally, numerous cell-based works are using G4 ligands without preliminary robust characterization of their G4-interaction properties, hence taking for granted that any G4 ligand is equivalent to another.

To clarify this situation, we undertook a systematic comparison of the most widely-used G4 ligands using three biophysical methods namely FRET-melting, G4-FID assay and SPR. To this purpose, we selected a set of 11 lead compounds representative of G4 targeting; in detail this panel is comprised of first-generation ligands widely used as G4-probes in biophysical, biochemical and cellular assays (PhenDC3, PDS, PDC (360A), RHPS4, BRACO19, NMM, Cu-ttpy) and of G4-drugs investigated in pre-and clinical trials (Quarfloxin, CX5461, c-PDS).[29, 34, 36, 55-57] The systematic comparison of the ranking obtained from the three methods in the presence of five G4 structures chosen as prototypes (22AG, 21CTA, 25CEB111, 25CEBwt, HIV-PRO1) allowed to classify ligands in groups based on affinity taking into account the limitations of each method and the drawbacks associated to some ligands (solubility, conflicting optical properties).[7, 58-61] The final goal of this study is to provide a robust guide for chemists and biologists as well as for newcomers in the field who may not have access to the required equipment. Of note, all selected ligands have shown high selectivity for G4 vs double-stranded DNA (except TMPyP4), hence our study focused exclusively on G4 affinity comparison.

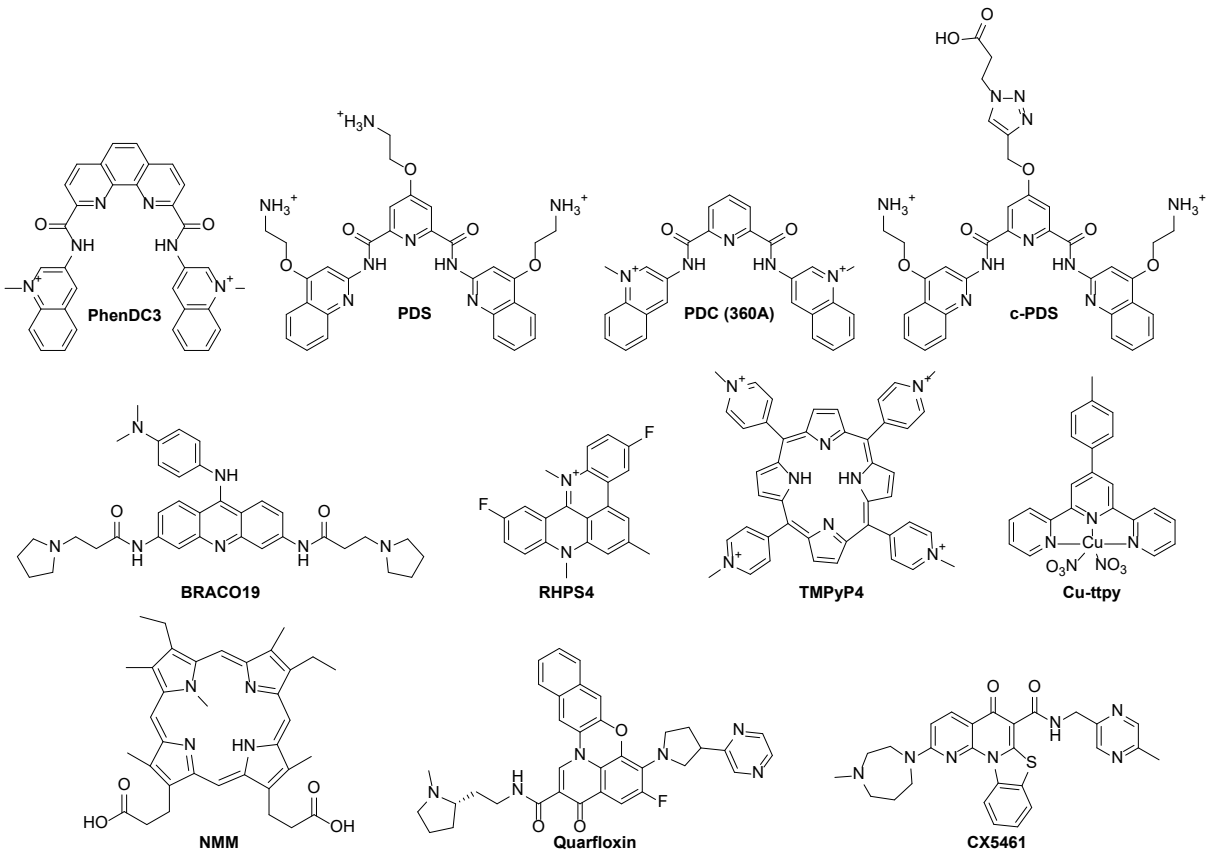

Figure 1. Structures of the G4 ligands chosen as benchmarks for this study, in parenthesis are indicated the estimated cationic charge at pH 7.2: PhenDC3 (3^+), PDS (2-3^+), PDC (360A) (2^+), c-PDS (1^+), BRACO19 (2^+), RHPS4 (1^+), TMPyP4 (4^+), Cu-ttpy (2^+), NMM (anionic 2^-), Quarfloxin, CX546 (1^+), CX5461 (1^+).

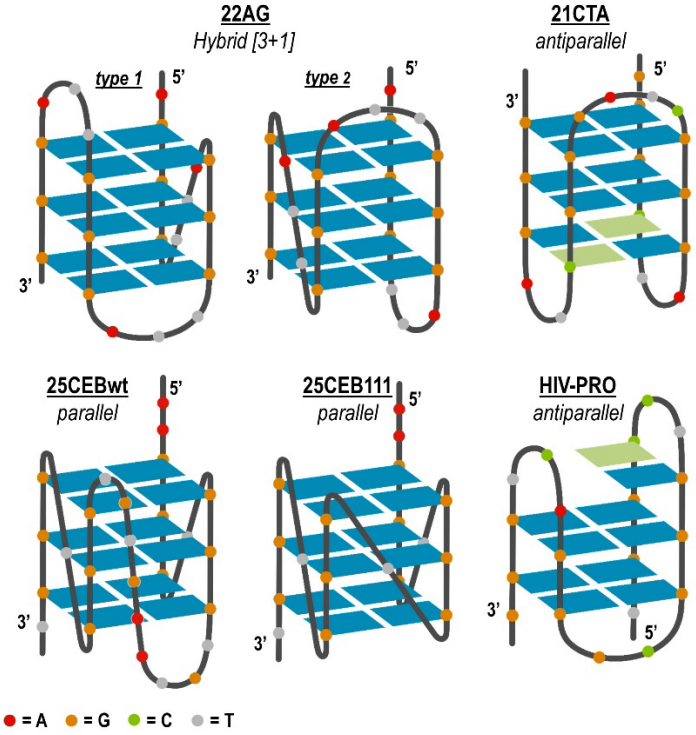

	Sequence	
22AG	5'-AGGGTTAGGGTTAGGGTTAGGG	Hybrid
21CTA	5'-AGGGCTAGGGCTAGGGCTAGGG	Antiparallel
25CEB111	5'- AAGGGTGGGTGGGTGGGT	Parallel
25CEBwt	5'-AAGGGTGGGTGTAAGTGTGGGTGGGT	Parallel
HIV-PRO1	5'- TGGCCTGGGCGGGACTGGG	Antiparallel

Figure 2. Top) Schematic representation of the G4 structures used for this study: 22AG as (3+1) hybrid topology, 21CTA and HIV-PRO1 as antiparallel topology, and 25CEB111 and 25CEBwt as parallel topology; bottom) Table showing names and corresponding G4 sequences.

Materials and methods

All commercially available chemicals were purchased from Sigma-Aldrich (PDS, BRACO19, TMPyP4, c-PDS), MedChemExpress (Quarfloxin), Selleckchem (CX5461), TOCRIS Bioscience (RHPS4), and Frontier scientific (N-Methyl Mesoporphyrin IX, NMM) as biochemical reagent grade and were used without further purification. PhenDC3,[62] PDC (initial name 360A),[63] Cu-ttpy[64] are in-house compounds that were synthesized as previously described. HS-$(CH_2)_{11}$-EG_6-Biotin and HS-$(CH_2)_{11}$-EG_4-OH were procured from Prochimia.TO-PRO3 and cacodylic acid were purchased from Aldrich and used without further purification. Stock solutions of TO-PRO3 (1 mM in DMSO) were used for G4-FID assay. Fluorescent probe powder and stock solution, divided in aliquots to avoid freeze–thaw cycles, were stored and used protected from light.

Oligonucleotide sequences used for FRET and G4-FID assays were purchased from Eurogentec as dried samples purified by RP-HPLC. 3'-biotinylated oligonucleotides for SPR studies were purchased from IDT and the other biomolecular systems (see supporting information) were prepared using the reported procedures.[52-53, 65] The dual fluorescently-labeled oligonucleotides bear as a donor fluorophore 6-carboxyfluorescein (FAM) in position 5' and as acceptor fluorophore 6-carboxytetramethylrhodamine (TAMRA) in position 3'. Oligonucleotides were dissolved in MilliQ water to a final concentration of

200 µM and stored at -20 °C. Concentrations were determined by absorption measurements at 260 nm at 95 °C using the molar extinction coefficient provided by the supplier.

Förster Resonance Energy Transfer (FRET)-melting assay

PhenDC3, PDS, PDC, RHPS4, TMPyP4, NMM and c-PDS were dissolved in DMSO to obtain solutions at 2 mM concentration and stored in the dark at -20 °C. Quarfloxin was dissolved in water at pH 5 to obtain a solution at 1.65 mM and CX5461 was dissolved in 50 mM sodium phosphate (pH 3.5) to obtained a solution at 2 mM as recommended by the supplier. Folded G4 structures were prepared as follows: G-rich sequences were heated at 95 °C for 10 min in appropriated buffer and left to fold at 4 °C overnight. Buffer conditions are specified below for each G4 sequence. FRET-melting assay was performed in Microamp Fast optical 96-well reaction plate (Applied Biosystems) on a real-time PCR apparatus, 7900HT Fast Real-Time PCR system. This assay was carried out in the presence of doubly-labelled fluorescent sequences (5'-FAM/donor and 3'-TAMRA/acceptor) 0.2 µM (1 molar equiv.) and G4 ligand 1 µM (5 molar equiv.) in a total volume of 25 µL. Solutions were prepared in buffer containing 10 mM lithium cacodylate, pH 7.2, and 10 mM KCl, completed by 90 mM LiCl for F21T and F21CTA and 1 mM KCl, completed by 99 mM LiCl for all the others G-quadruplex sequences. The FAM channel was used to collect the fluorescence signal. Stabilization of compounds with G4 structures was monitored with this method: 5 min at 25 °C and then increase of 0.5 °C every minute until reaching 95 °C. The stabilization was evaluated by determining the temperature at half denaturation of the G4 (obtained at the half height of the sigmoidal curve, $\Delta T_{1/2}$) in the absence and in the presence of ligand. A series of five oligonucleotides covering a range of possible G4 conformations was used (Table S1).

High-Throughput G4 Fluorescent Intercalator Displacement assay (HT-G4-FID)

Folded G4 structures were prepared as follows: The sequences at 5 µM concentration were heated at 95 °C for 10 min in K^+100 (10 mM lithium cacodylate (pH = 7.2) and 100 mM KCl) and left to fold in ice for 30 min. TO-PRO3 was added to the solution to a final concentration of 10 µM.

G4 FID assay was performed on a FLUOstar Omega microplate reader (BMG Labtech) in 96-well plate Non-Binding Surface black with black bottom polystyrene microplates (Corning). The microplate was filled with (a) K^+100 buffer (qs for 200 µL), (b) 10 µL of a solution of pre-folded oligonucleotide (5 µM, 1 mol equiv.) and fluorescent probe (TO-PRO3 (10 µM, 2 mol equiv.)), and (c) increasing volumes of a freshly prepared 5 µM ligand solution in K^+100 buffer (0, 5, 10, 15, 20, 25, 30, 40, 50, 60, 80, 100 µL) along the line of the microplate, *i.e.* from column A to column H the concentration of the ligand will be: 0, 0.125, 0.25, 0.375, 0.5, 0.625, 0.75, 1.0, 1.25, 1.5, 2.0, and 2.5 µM respectively. After 5 min of orbital shaking at 500 rpm, fluorescence is measured using the following acquisition parameters: positioning delay of 0.5 s, 20 flashes per well, emission/excitation filters for TO-PRO3 at 620/670, gain adjusted at 80% of the fluorescence from the most fluorescent well. TO-PRO3 displacement is calculated from the fluorescence intensity (F):

$$TO\text{-}PRO3\ displacement = 1 - \frac{F}{F_0}$$

where F_0 is the fluorescence of TO-PRO3 bound to DNA without G4 ligand. TO-PRO3 displacement is then plotted as a function of the concentration of the added G4 ligand. G4 affinity was evaluated by the displacement of TO-PRO3 at 1 µM G4 ligand concentration, after non-linear fitting of the displacement curve. A series of five oligonucleotides covering a range of possible G4 conformations was used (Figure 2 bottom).

Surface plasmon resonance (SPR)

PhenDC3, PDS, PDC, RHPS4, TMPyP4, NMM and c-PDS were dried and stored in the dark at -20 °C. These compounds were dissolved directly in the SPR running buffer, immediately before the experiments, at the desired maximum concentration (Table S5), followed by serial dilutions using the SPR running buffer. Quarfloxin and CX5461 were initially dissolved in 100% DMSO to yield concentrations of 1.32 mM and 2.92 mM, respectively. These solutions were then diluted in an SPR running buffer containing DMSO to ensure that each tested ligand concentration maintained a 5% DMSO concentration. Cleaning procedure of the gold sensor chips included UV-ozone treatment during 10 min followed by rinsing with MilliQ water and ethanol. The cleaned gold surfaces were then functionalized according to the following procedure. Firstly, mixed self-assembled monolayers (SAMs) were formed at room temperature by dipping overnight gold sensors in the thiol mixture: 80% HS-$(CH_2)_{11}$-EG_4-OH and 20% HS-$(CH_2)_{11}$-EG_6-Biotin (1 mM total thiol concentration in EtOH). After overnight adsorption, gold sensors were rinsed with ethanol and dried under nitrogen. The surface was then inserted in the BIAcore T200 device. All measurements were performed at 25 °C, using a running buffer (RB) composed of HEPES buffered saline: 10 mM HEPES pH 7.4, 50 mM NaCl, 100 mM KCl and 0.05% *v/v* surfactant P20 (5% DMSO was added for the study of interactions with CX5461 and Quarfloxin ligands). Streptavidin (100 ng/mL) was injected (10 µL/min) on the biotinylated SAM until saturation of the surface (around 2400 RU). The different oligonucleotides were injected at 2 µL/min on streptavidin-coated SAM surfaces until surface saturation (between 200 and 350 RU).

Binding experiments were conducted on G4 ligands (Figure 1) at 30, 80 or 100 µL.min^{-1} by injection of the G4 ligands dissolved in RB at five or ten different concentrations using a single cycle kinetic method. The experimental parameters applied to each G4 ligand are given in Table S5. A streptavidin surface, prepared as described below, was used as reference. Signals from the curves obtained on the reference surface were subtracted from the curves recorded on the recognition surfaces, allowing elimination of refractive index changes due to buffer effects. The solvent correction procedure was also applied with the G4 ligands dissolved in DMSO. The equilibrium dissociation constants were determined mainly by the fitting of the Langmuir isotherm from the response at the equilibrium state except for PhenDC3, for which the K_D value was calculated from the binding rate constants as $K_D = k_{off}/k_{on}$ (k_{off} represents the dissociation kinetic constant and k_{on} represents the association kinetic constant) because the equilibrium was not reached. The reported values are the mean of representative independent experiments and the errors provided are standard deviations from the mean. Each SPR experiment was repeated at least three times.

Results

Förster Resonance Energy Transfer (FRET)-melting assay

Firstly, the binding properties of the selected G4 ligands were studied by Förster resonance energy transfer (FRET) melting assay. For this purpose, we chose as prototype five DNA sequences which structures are fully characterized: the human telomeric sequence (F21T), the human telomeric sequence antiparallel variant (F21CTAT), the human minisatellite repeat native sequence 25CEBwt (F25CEBwtT) and modified sequence 25CEB111 (F25CEB111T), and the HIV 1 promoter sequence HIV-PRO1 (FHIV-PRO1T) (Table S1).[7, 58-61] All sequences are optimized and doubly-labelled with FRET fluorophores partners (5'-F(FAM/donor) and 3'-T(TAMRA/acceptor) as highlighted in the name) to follow the unfolding of the G4 structures as function of temperature (Figure S1). This assay was carried out in the classical conditions optimized by Mergny *et al*.[40]: 0.2 µM of G4-DNA in the presence of 1 µM (5 molar equiv.) of G4 ligand in potassium-containing buffer (conditions specified in Table

S2). As reported in previous studies, we were unable to test RHPS4 by FRET-melting assay due to the overlap of its emission spectrum with that of FAM.[66] As expected, the amplitude of the stabilization induced by the ligand ($\Delta T_{1/2}$) can be correlated to the melting temperature of the targeted G4 alone that in turn depends on its structure and sequence (Figure 3, Table S2). However, we could clearly identify specific trends and outliers common to all the G4 studied sequences. In the presence of the human telomeric sequence (F21T) that is polymorphic (mix of hybrid structures), PhenDC3, PDS, PDC and TMPyP4 displayed very strong stabilization properties with $\Delta T_{1/2}$ values ranging from 30 to 27.9 °C, followed by BRACO19 with $\Delta T_{1/2}$ of 19.3 °C. On the opposite, Quarfloxin, CX5461, and c-PDS showed $\Delta T_{1/2}$ values below 7.9 °C indicating weak binding. A similar trend was observed with the antiparallel structure F21CTAT and the parallel G4 characterized by a 9-nucleotide central loop F25CEBwtT (Figures S1): PhenDC3 and TMPyP4 outperformed all the ligands with $\Delta T_{1/2}$ values of 19.0 and 24.2 °C respectively, PDS, PDC and BRACO19 showed similar behaviour with $\Delta T_{1/2}$ values comprised between 13.4 and 11.2 °C and 16.5 and 13.6 °C, respectively. Again, the G4-drugs investigated in pre-and clinical trials Quarfloxin, CX5461, and c-PDS revealed weak binding showing $\Delta T_{1/2}$ below 2.5 °C. Of note, the three G4 sequences above (F21T, F21CTA, F25CEBwtT) show similar melting temperature values in the conditions applied ($T_{1/2}$ around 55 °C), hence the $\Delta T_{1/2}$ values induced by the ligands can be compared significantly from one G4 to another (see Table S2). In that sense, the data indicate clearly that the telomeric G4 F21T is more strongly bound than F21CTAT and F25CEBwtT, whereas stabilisation values are almost at the same level for the latter two. In the case of the parallel structure F25CEB111T, that is highly stable with a $T_{1/2}$ of 71.5 °C in our conditions (1 mM K^+), lower stabilisation values were obtained as expected, preventing comparison with the three above-mentioned G4s. Nonetheless, globally the same trend is observed within the panel of ligands: The top 4 high affinity ligands are PhenDC3, PDS, PDC and TMPyP4 which displayed $\Delta T_{1/2}$ in the same range (17.3 °C < $\Delta T_{1/2}$ < 13.0 °C) and are followed by BRACO19 with a slightly lower $\Delta T_{1/2}$ (9.3 °C). Once again no measurable effect was observed with the three preclinical G4-drugs. The FHIV-PRO1T G4 deviates somewhat from the profiles observed for the four previous sequences. Particularly low stabilization values were observed for the top ligands ($\Delta T_{1/2}$ for PhenDC3 = 9.5, $\Delta T_{1/2}$ for PDC = 7.4 °C) partly explained by the high $T_{1/2}$ (61 °C) but also, and most likely, due to the particular antiparallel G4 structure of this sequence comprised of two G-quartets with an additional Watson-Crick CG base pair. Surprisingly, TMPyP4 induced a remarkably high temperature increase ($\Delta T_{1/2}$ = 20.9 °C) suggesting a potent interaction possibly with a strong contribution of electrostatic forces since TMPyP4 is highly charged (4+) as compared to the other ligands (Figure 1). Despite this unexpected result, for the rest of the series, the ligands can be split in the same two groups as previously observed: PhenDC3, PDS, PDC and BRACO19 exhibiting $\Delta T_{1/2}$ ranging from 12.9 and 7.4 °C and Quarfloxin, CX5461, and c-PDS with $\Delta T_{1/2}$ below 4.8 °C (down to 1.7 °C for CX5461). Finally, two ligands showed a heterogeneous behaviour escaping the trend: the first one is Cu-ttpy that stabilizes strongly and specifically the human telomeric sequence with a $\Delta T_{1/2}$ of 20.4 °C whereas $\Delta T_{1/2}$ values below 5 °C are observed for the other G4 structures. The second one is NMM that exhibited an almost complete lack of effect with all sequences ($\Delta T_{1/2}$ <1.3 °C or not measurable).

The data of FRET-melting allow to make a reliable affinity ranking of ligands and easily discriminate between strong and weak binders provided that the ligands studied do not significantly interfere with the fluorescence of the probes labelling the G4 sequences. However, the main issue of FRET-melting assay resides in the difficulties to compare $\Delta T_{1/2}$ values induced by ligands from one G4 sequence to another since by definition $T_{1/2}$ (and thus $\Delta T_{1/2}$) are values relative to each G4 structure in given conditions. This issue is illustrated by the two examples above (F25CEB111T and FHIV-PRO1T) meaning that stabilization values ($\Delta T_{1/2}$) should be handled with care when used for a purpose of comparison. Finally, the data emphasize the importance of benchmarking the assay with one or two

reference compounds with well-characterized G4 binding behavior (typically PhenDC3 or PDS, PDC). This should not only allow to identify deviant behaviors of G4 targets or of G4 ligands but also this can be of practical interest to evaluate the order of magnitude of the apparent binding affinity (K_D) for new ligands. The K_D of PhenDC3 for the telomeric G4 has been previously determined by SPR, which showed a value in the nanomolar range,[53] thus one could ask if PhenDC3 exhibits such an outstanding affinity with the other G4s and also to which extent K_D values vary within the group of top ligands classified as strong stabilizers and with regard to the group of weak stabilizers.

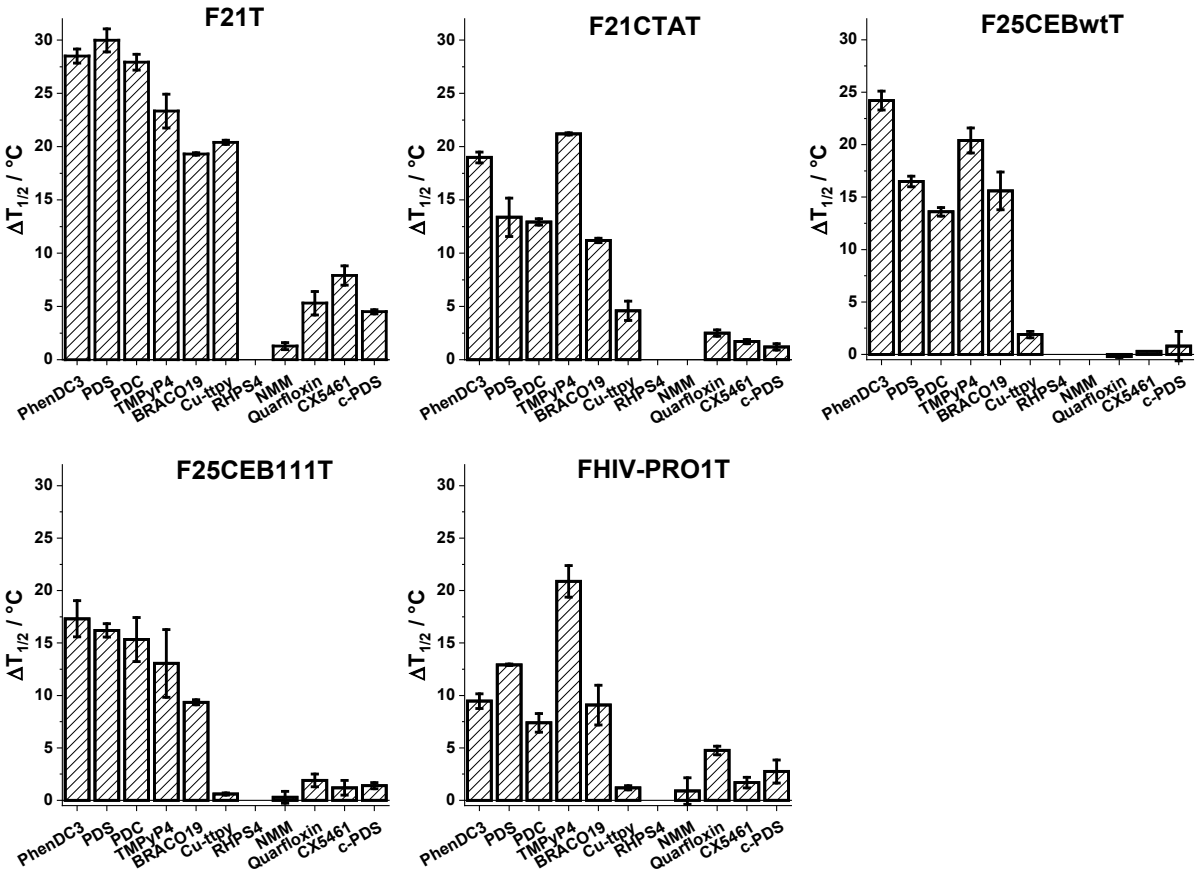

Figure 3. FRET-melting experiments in the presence of human telomeric sequence F21T, human telomeric sequence variant F21CTAT, human minisatellite repeat native sequence F25CEBwtT, human minisatellite repeat modified sequence F25CEB111T, and HIV1 promoter sequence FHIV-PRO1T. [G4-DNA] = 0.2 µM, [ligand] = 1 µM;, buffer: lithium cacodylate buffer (10 mM, pH 7.2), 10 mM KCl + 90 mM LiCl for F21T and F21CTAT, and lithium cacodylate buffer (10 mM, pH 7.2), 99 mM LiCl + 1 mM KCl for all the other sequences. Error bars corresponds to SD of three independent experiments. *RHPS4 is not compatible with this assay, see text.[66]

High-throughput G4 Fluorescent Intercalator Displacement assay (HT-G4-FID)

The second method we used to study the binding affinities of the G4 ligands and the five prototype G4 structures was the high-throughput G4 ligand fluorescent intercalator displacement assay. We carried out a titration experiment at increasing G4 ligand concentration in the presence of the unlabelled aforementioned G4 sequences (Figure 2) and by following the experimental conditions optimized by Teulade-Fichou *et al.*[41]: 0.25 µM of G4 structure, 0.5 µM (2 molar equiv.) of fluorescent probe in potassium containing buffer (Figure S2). Of note, since TO emission may overlap with some ligands (*e.g.* TMPyP4), TO-PRO3 was used instead, its fluorescent emission spectrum being compatible with all G4 ligands selected for this study. Since several ligands were not able to displace 100% of TO-PRO3 even at high concentration, the corresponding DC_{50} (concentration of G4 ligand required to displace

50% of TO-PRO3) cannot be determined.[41] Therefore the binding affinity indicator used was the displacement of TO-PRO3 at 1 µM ligand concentration (TO-PRO3D)[41] expressed as the percentage (%) of displacement normalized to 1. The results are summarized in Table S3 and represented as bar graphs in Figure 4. A supplementary advantage of using this indicator is that we operate in conditions nearly similar to that of the FRET-melting assay (ligand to G4 ratio 1/4 vs 1/5, [G4] 0.25 µM vs 0.2 µM), which facilitates comparison of data obtained with the two assays. The first straightforward observation is that PhenDC3 is able to displace TO-PRO3 with remarkably high efficiency from 22AG, 21CTA, 25CEB111, and 25CEBwt (0.84 <TO-PRO3D< 0.96) indicating strong binding without clear preference for a specific G4 topology. In the range below (0.63 <TO-PRO3D< 0.85), we found the 4 other top ligands namely PDC and PDS, BRACO19 and TMPyP4, indicating a strong interaction with the four G4 sequences but with a slightly lower strength than PhenDC3. However, PDS escaped somehow this trend in two cases (21CTA and 25CEBwt) for which a TO-PRO3D value close or below 0.5 was measured (0.54 and 0.47 respectively), thus indicating a more discriminative behaviour as function of the G4 structure than the other top ligands. In this assay,[41] displacement values above 0.60 characterizes "high affinity binders" thus the data obtained herein are globally consistent with the top 5 ligands identified in the FRET-melting assay. Interestingly, RHPS4 that could not be evaluated by the FRET-melting assay appeared to bind significantly with TO-PRO3D values similar to TMPyp4 for the two telomeric sequences (0.62, 0.56 for 22AG and 21CTA respectively) but clearly lower for the two minisatellites sequences (0.32 and 0.29 for 25CEBwt and 25CEB111 respectively), indicating a strong to moderate binding strength (0.62<TO-PRO3D< 0.29). Of note, G4-FID data for Cu-ttpy are not consistent with the strong preference for telomeric G4 observed by FRET-melting as binding rather independent of the G4 structure is shown with performances slightly below as compared to the top group (0.67 <TO-PRO3D< 0.46). Conversely, in line with the FRET-melting data, NMM showed low binding affinity, with TO-PRO3D < 0.1 in most cases, this ligand is a bit more active on 25CEBwt while remaining at low level (TO-PRO3D = 0.24). Finally, the behaviour of ligands for binding HIV-PRO1 is again particular. Consistent with FRET-melting, TMPyP4 displayed a high binding with a TO-PRO3D of 0.73 and all other compounds (PDC, BRACO19, Cu-ttpy, RHPS4) showed a significantly weak affinity with TO-PRO3D lower than 0.40, down to 0.07 for RHPS4. Of note PhenDC3 appeared significantly more efficient as compared to its FRET-melting performance ranking at the same level as TMPyP4 (TO-PRO3D = 0.74), see curves Figure S2. Intriguingly, we were unable to study the interaction between PDS and HIV-PRO1 due to increase of TO-PRO3 fluorescence during titration (Figure S2). This phenomenon was also observed with Quarfloxin, CX5461 and c-PDS but with all G4-sequences indicating that these ligands are unable to induce probe displacement even at a 10-fold higher concentration. Partial displacement of TO-PRO3 may indeed occur but at much higher ligand concentration (100-fold) (Figure S3). This fluorescence enhancement is artefactual and suggests a complex dynamic interplay between TO-PRO3, (free and bound), the ligand and the G4.

We see that G4-FID and FRET-melting are globally consistent for ligand ranking with regard to each G4 sequence as illustrated by Figures 3 and 4. The panel divides in two groups: the top ligands (PhenDC3, PDC, PDS, BRACO19, TMPyp4) with PhenDC3 as lead compound as clearly seen from the TO-PRO3 displacement curves (Figure S2) and the low activity ligands (CX5461, c-PDS, Quarfloxin, Figure S3). In addition the G4-FID provided complementary information in allowing evaluation of RHPS4 which is positioned in between the two groups as clearly seen from titration curves (Figure S2). Although inconsistencies appear due in part to the limitations and constraints of each assay, these points out to the particularity of ligands for instance Cu-ttpy is a metallic complex that may establish electrostatic or coordination interactions likely to impact the melting.

The proper interpretation of G4-FID data requires to know the precise interaction of the fluorescent probe with the analysed G4 structures since the test is more reliable if the probe and the ligand compete for the same binding site.[41] The binding constants of TO-PRO3 for a panel of G4s have been previously determined and shown to fall in the micromolar range (K_D) with minor variations from one G4 to another (for instance the log K_A of TO-PRO–3 for 22AG and 21CTA are 6.3 and 6.5 M^{-1} respectively) thus making the comparison of data obtained with the studied oligonucleotides significant. In other words the principle of the test being based on the competitive displacement of TO-PRO3, it allows to estimate roughly a K_D threshold for the ligand/G4 interaction: Globally in the conditions applied (low G4 concentration, small excess of ligand ligand/ G4 =5) efficient ligands should have a K_D value below micromolar and consequently poorly to non-active ligands have K_D around the micromolar range or above.

Thus as previously addressed for FRET-melting, the question arises: can we estimate that ligands with efficacy similar to PhenDC3 (TO-PRO3D > 0.8-0.9) have nanomolar K_D or to which extent the K_D varies within the top group ligands showing TO-PRO3D between 0.9 and 0.6 (90-60% probe displacement). Conversely to which extent ligands discarded in the conditions of the FID-assay are able to bind G4?

In other words, based on the two semi-quantitative indicators collected by FRET-melting and G4 FID, would it be possible to make a reliable estimation of K_D, at least of the order of magnitude, for a given ligand/G4 pair? If established, this approach would provide a simple guideline for rapid binding affinity evaluation of new potential G4 ligands.

To address the question, a third method based on quantitative determination of affinity was needed, this is why the same panel of ligands and G4 sequences was investigated by using SPR.

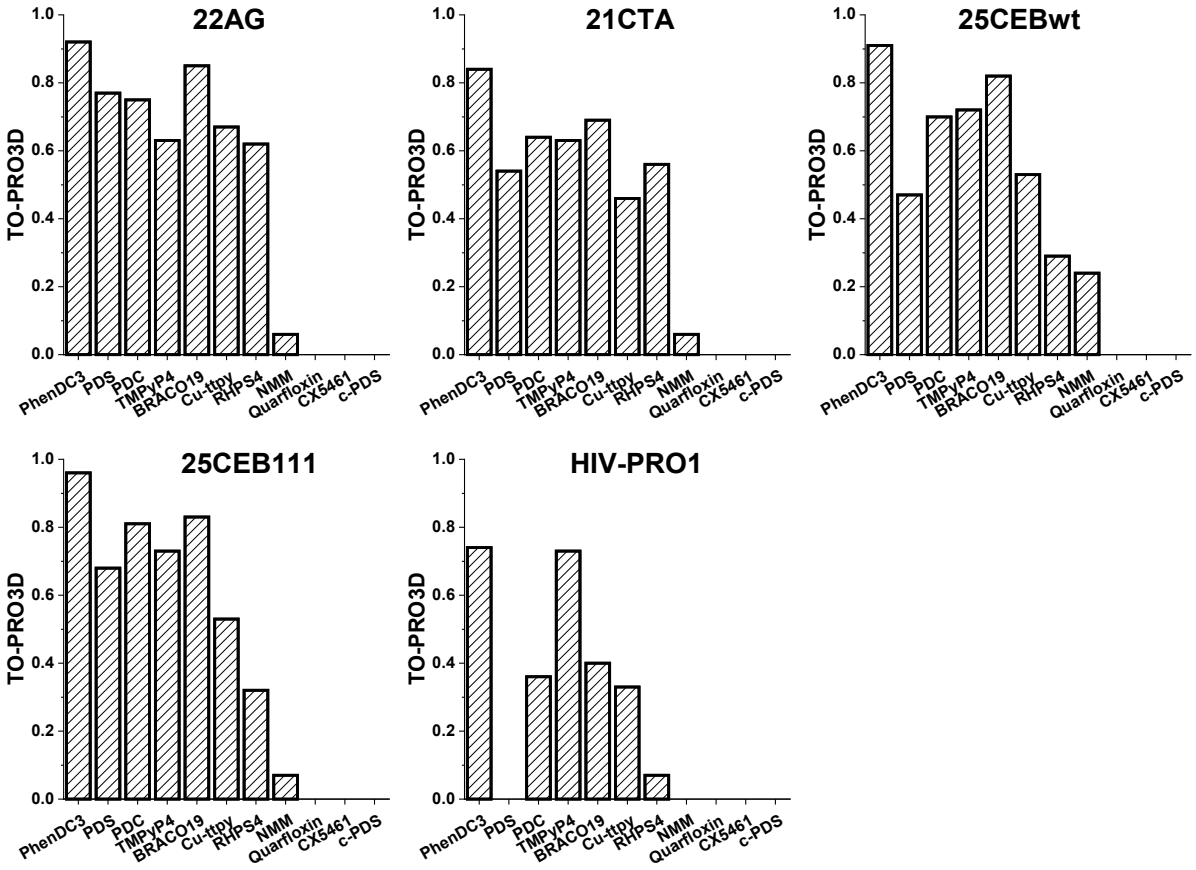

Figure 4. Bar charts representing TO-PRO3 displacement at 1 μM of G4 ligand concentration. G4 structure concentration 0.25 μM and TO-PRO3 concentration 0.5 μM in 10 mM lithium cacodylate buffer (pH 7.2) and 100 mM KCl. Quarfloxin, CX5461, c-PDS do not displace TO-PRO3 from all G-quadruplex structures and PDS do not displace TO-PRO3 bound to HIV-PRO1. TO-PRO3D values are obtained after non-linear fitting of the displacement curve generated by two independent experiments.

Surface plasmon resonance (SPR) binding analysis

The third method used to determine the binding affinities of the ligands for the G4 targets was the surface plasmon resonance (SPR). This quantitative technique has been regularly used in the field for accurate determination of the thermodynamic and kinetic constants of interactions between ligands and G4 targets.[67-69] As for FRET-melting and G4-FID, the SPR technique does not require special radioactive or fluorescent labelling of the ligands to be analysed, is highly sensitive and uses very low quantity of ligands and G4-targets. To perform the analysis, a combination of biotinylated sequences (22AG, 25CEBwt, 25CEB111) and topologically constrained variants synthesized on a cyclic peptide scaffold (22AG, 21CTA, 25CEB111, HIV-PRO1) were used, the latter have been previously reported for exploring G4 ligands binding via SPR (Table S4 and Figure S4).[52-53, 65] The sequences were immobilized onto streptavidin SAM layer and five increasing concentrations of the G4 ligands were injected using the single cycle kinetic (SCK) method. The concentration ranges for each ligand were adjusted based on preliminary measured affinity. This was done to ensure that the concentration ranges spans over 0.1 and 10 times the K_D values. For Cu-ttpy, Quarfloxin and c-PDS, two different ranges of concentrations were injected to allow for a better determination of the affinity. The sensorgrams are presented in Figures S5 to S63. The sensorgrams obtained for TMPyP4, RHPS4, BRACO19, PhenDC3, PDS, and PDC exhibited a typical pattern, where the signal increased with increasing ligand concentration and reached a maximum amplitude signal between 20 and 100 RU (Response Units) which is fully consistent with the amount of immobilized G4, the optical properties ratio (refractive index increment, RII), the molecular weight of the ligand, and an interaction valency between 1 and 2.[70-71]. Among these ligands, some sensorgrams showed that the signal returned close to the baseline after the washing step with RB, indicating complete dissociation between the G4 and the ligand. However, for others such as PhenDC3 and PDS, the signal after RB washing step remained well above the baseline, indicating an incomplete dissociation between the G4 and the ligand. Non-conventional sensorgram shapes or amplitudes were observed for c-PDS, CX5461, Quarfloxin, and Cu-ttpy. In the cases of c-PDS, CX5461, and Quarfloxin, the signal exhibited unusually high amplitudes, reaching 500 RU, 3500 RU, and 2500 RU, respectively. The elevated signal amplitude observed with these ligands could potentially be attributed to modifications in the G4 conformations or ligand aggregation occurring at high concentrations. Further investigation would be required to better understand the underlying causes of these atypical sensorgram characteristics. It is important to note that while total dissociation was observed during the washing step for the three ligands, subsequent analysis on the same G4 chips was prevented due to signal perturbations. This applied regardless of the specific ligand being investigated in the subsequent analysis. In the case of Cu-ttpy, the sensorgrams did not consistently exhibit concentration dependence. Additionally, they displayed a high response amplitude, as mentioned before, along with low reproducibility of the response at certain concentrations, such as for 25CEBwt and 22AG. These signal disturbances observed for all four ligands could potentially be attributed to ligand precipitation during the analysis.

All the sensorgrams obtained for the various G4 binders exhibited a plateau at the end of the injection time, except for PhenDC3. Consequently, the determination of all affinity constants relied on the response at steady-state equilibrium through the fitting of the Langmuir isotherm (as shown in Figure S5 to S63). In the case of PhenDC3, the K_D value was determined using the kinetic constant (K_D =

k_{off}/k_{on}, where k_{off} represents the dissociation kinetic constant and k_{on} represents the association kinetic constant). All K_D values correspond to fitting with a 1/1 model.

The K_D values obtained from the various G4s and ligands were expressed in pK_D units (*i.e.* log K_A) for the purpose of easy comparison within SPR data and with FRET-melting and G4-FID data (Figure 5 and Table1 and S6). In cases where two pK_D values were determined for the same sequence, with one obtained from the biotinylated sequence and the other from the topologically constrained sequence, an average pK_D value was calculated. This average pK_D value was then utilized for visual representation and subsequent discussion. These values, including those with non-conventional behavior, are summarized in Table 1 and S6 and represented as bar graphs in Figure 5. However, it is important to take care when interpreting certain affinity values, particularly for c-PDS, CX5461, Quarfloxin, and Cu-ttpy due to the issues explained above.

The most straightforward observation is that PhenDC3 exhibits remarkable affinity for all G4 targets, as evidenced by the high pK_D values determined ($8.6 < pK_D < 9.7$). Notably, this strong binding is not related to a specific G4 topology. Then the group of strong binders previously identified in FRET and FID could be divided in two subgroups: i) the first one is constituted by PDS and PDC which are found in the range just below PhenDC3 ($7.1 < pK_D < 8.1$); and also exhibit high affinities with minimal variability across the different G4 targets; ii) the second one comprises TMPyP4, BRACO19 and RHPS4 in the range of one pK_D unit lower ($6.2 < pK_D < 7.2$). In this subgroup, there is a moderate to significant variation across the G4 targets indicating a slight preference of the three ligands for the two parallel G4 structures (25CEBwt, 25CEB111) as compared to antiparallel one (21CTA), the pK_D values were increased of 0.2-0.5 for TMPyp4; 0.6-1 for BRACO19 and 0.2-0.4 for RHPS4. Finally, for the group of compounds classified as weak binders (CX5461, Quarfloxin c-PDS), pK_D values between 4.5 and 5.3 were determined with the sole exception of 21CTA for which a too weak interaction prevented K_D measurement (Table 1 and S6). Interestingly, K_D values determined for HIV-PRO1 are positioned exactly in the pK_D intervals described above thus evidencing the high binding of PhenDC3 ($pK_D = 8.8$), the strong interaction of PDS and PDC ($pK_D = 7.5$ in both cases) and strong to moderate binding for the subgroup TMPyp4, BRACO19, RHPS4 (pK_D = 5.9, 7.1, 6.1 respectively). Again, and similarly to 21CTA, the affinity constant could not be determined for the group of weak binders, which suggests that the two antiparallel G4 structures are significantly more difficult to be bound.

Collectively the SPR measurements confirm the K_D estimation derived from G4-FID data, presumed strong binders have indeed K_D below micromolar ($pK_D > 6$) and weak binders have K_D above micromolar ($pK_D < 6$). Of note the values determined herein are in agreement with data already published.[50, 53-54, 72] However, careful examination of the K_D values evidences the very large differences existing between the two groups since a variation of up to 5.5 order of magnitude in K_D is measured between the strongest interaction (pK_D PhenDC3/25CEB111= 9.75) and the weakest (pK_D CX5461/25CEBwt = 4.4). As well, within the group of strong binders the pK_D variation is spanning a range of 3.5 unit (pK_D PhenDC3/25CEB111= 9.75, pK_D TMPyp4/21CTA = 6.2). It is clear that these considerable differences should impact the capacity of ligands for targeting G4 in complex media and therefore should be considered in biological applications.

SPR results helped to better understand the particular cases observed by the two other methods above: *i)* SPR analysis allows the measurements of the interaction between NMM and all G4 targets, demonstrating strong affinity with parallel G4 structures (pK_D 7.2 and 7.05 for 25CEB111 and 25CEBwt, respectively). As already reported, NMM deviates from the trend of uniform binding affinities exhibiting significantly lower binding for the hybrid G4 structure 22AG ($pK_D = 5.2$) whilst no K_D values could be determined for the antiparallel G4 structures 21CTA and HIV-PRO1 due to weak

interaction signals.[52, 73] The preferential high binding to parallel G4 is not observed by FRET-melting and G4-FID, as NMM fails to strongly stabilize the two 25CEB G4 structures or efficiently displace TO-PRO3. Obviously the issues encountered herein are partly attributable to the poor solubility of this highly hydrophobic molecule which makes difficult its use in high-throughput screening conditions (stock solutions, DMSO storage, automated dilution, sticking to walls of settings); *ii)* in the case of Cu-ttpy, the pK_D values fall in the range 4.7 to 5.2 and no K_D could be determined for HIV-PRO1 which ranks this ligand in the group of low affinity binders. The preferential interaction for the telomeric G4 observed by FRET-melting and previously detected by ESI-MS is not confirmed by SPR.[74] This discrepancy points again to the chemical nature of this compound since it is notorious that metallic complexes are hardly compatible with storage in DMSO and may form aggregates. Moreover, copper(II) complexes are highly prone to establish electrostatic and coordination interactions with phosphates and heteroatoms of nucleic bases which may significantly affect G4-melting measurements through non-specific binding to unfolded forms and /or to G4-loops;[47] iii) the last case concerns PDS that exhibits high affinity for all G4 targets according to SPR and in agreement with FRET-melting data whereas its behavior is more heterogeneous in G4-FID. This suggests that the apparent absence of binding to HIV-PRO1 and the low activity with 25CEBwt detected in G4-FID (Figure 4) may not be genuine but rather a methodological bias. However, the low FID response of PDS with G4 harboring long loops has been reported already (*e.g.* with Bcl2 see J. Lefebvre PhD Thesis 2017, https://www.theses.fr/2017SACLS536). Hence since both 25CEBwt and HIV-PRO1 have respectively long lateral loops (25CEBwt, Bcl2) or a GC base pair (HIV-PRO1) surrounding the 3' external G-quartet, this response may indicate a highly dynamic interaction involving TO-PRO3, loops and PDS thereby preventing probe displacement and directing PDS to an allosteric site making it a false negative.

	22AG average	**21CTA-R**	**25CEBwt-b**	**25CEB111 average**	**HIV-PRO1-R**
PhenDC3	*9.05 ± 0.15*	*8.6 ± 0.1*[a]	*9.1 ± 0.1*	9.75 ± *0.25*	*8.8 ± 0.2*[b]
PDS	*7.15 ± 0.2*	*7.9 ± 0.3*[a]	*7.4 ± 0.1*	7.3 ± *0.2*	*7.5 ± 0.1*[b]
PDC	*7.4 ± 0.2*	*7.6 ± 0.2*	*8.1 ± 1.4*	7.9 ± *0.35*	*7.5 ± 0.2*
TMPyP4	*6.5 ± 0.2*	*6.2 ± 0*[a]	*6.4 ± 0.3*	6.75 ± *0.3*	*5.9 ± 0.3*[b]
BRACO19	*6.7 ± 0.1*	*6.5± 0.1*[a]	*7.1 ± 0.2*	7.5 ± *0.3*	*7.1 ± 0.1*[b]
RHPS4	*6.5 ± 0.15*	*6.8 ± 0.1*	*7.2 ± 0.3*	7.05 ± *0.25*	*6.1 ± 0.3*
Cu-ttpy	*4.7 ± 0.3*	*4.8 ± 0.2*	*5 ± 0..3*	5.25 ± *0.55*	ND**
NMM[c]	*5.2 ± 0.3*	ND* [c]	*7.2 ± 0.1* [c]	7.05 ± *0.2*	ND*
CX5461[d]	*4.5 ± 0.2*	ND**	*4.4 ± 0.3*	4.5 ± *0.9*	ND**
Quarfloxin[d]	*5 ± 0.2*	ND**	*5.1 ± 0.2*	5 ± *0.1*	ND**
c-PDS[d]	*5.4 ± 0.15*	*5.3 ± 0.1*	*5.5 ± 0.4*	5.25 ± *0.4*	ND**

Table 1. pK_D values obtained for each G4 ligand injected on the five prototypal G4 structures immobilized on the SPR sensor. Error corresponds to SD of at least three independent experiments.

ND*: not determined as the interaction was too weak for the sensorgram to be fitted with accuracy in order to obtained the kinetic data of the interaction.

ND**: not determined as non-conventional sensorgram shapes or amplitudes were observed

[a]: data already published in Bonnat et al.[53]

[b]: pK_Ds are consistent with previously published values in Bonnat et al.[53] .

[c]: data already published in Perrenon et al.[52]

[d]: The signals displayed irregular shapes or amplitudes, indicating that the pK_D values should be interpreted with caution.

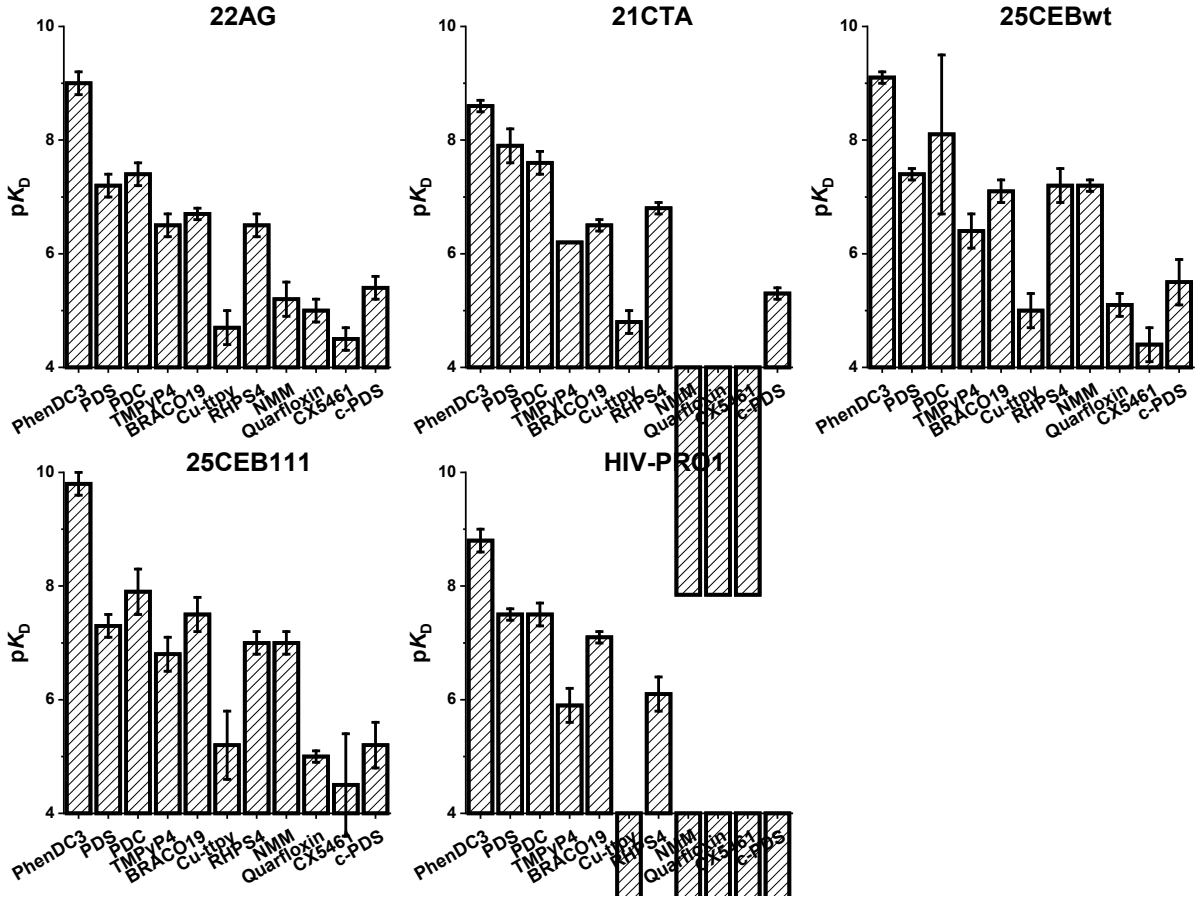

Figure 5. Bar charts representing pK_D or logK_A interaction between the immobilized G4 structures and the selected G4 ligands. For NMM/21CTA and NMM/HIV-PRO1 interactions, the pK_D value could not be determined as the sensorgram could not be suitably fitted to obtain the kinetic data of the binding due to weak interactions. For the interactions of Quarfloxin, CX5461 and c-PDS with 21CTA and HIV-PRO1, the pK_D value could not be determined as the sensorgram could not be suitably fitted due to unconventional signals. pK_D values are the means of three independent experiments obtained after fitting of the Langmuir isotherm from the response at the equilibrium state except for PhenDC3, for which the K_D value was calculated from the binding rate constants generated.

Discussion

In the whole, the SPR data allow to establish a dependable ranking of ligands based on their affinity and effectively differentiate between strong and weak binders. This holds true as long as the ligands adhere to the experimental requirements, such as compatibility with microfluidics, buffer solubility, and concentration-dependent response. Notably, we observed that the SPR data globally align with the rankings obtained from FRET-melting and G4-FID methods for evaluating ligands against each G4

target. PhenDC3 emerges as the most potent binder among all G4 targets, which is in line with its strong ability to displace TO-PRO3 and stabilize all G4 structures. As seen in FRET-melting and G4-FID, four other prominent ligands namely PDC, PDS, BRACO19, and TMPyP4 exhibit high affinity towards most G4 targets under investigation, with minimal pK_D variations across the different G4 targets. On the other hand, ligands such as Quarfloxin, CX5461, and c-PDS, which fail to stabilize G4 structures in FRET-melting and do not displace TO-PRO3 in G4-FID, demonstrate weak to undetectable binding in SPR. Remarkably, for all the ligands/G4 complexes mentioned above, it exists a clear correlation between the semi-quantitative indicators obtained from FRET-melting and G4-FID, and the quantitative affinity measured through SPR, as shown by the 3D scatter plot reported in Figure S64. The order of magnitude of the interactions remains consistent across all three techniques. This consistency might be attributed to the fine-tuning of parameters employed in FRET-melting and G4-FID experiments, such as low G4-DNA concentration and moderate ligand excess, which effectively highlight differences in binding capacities.

However, a complete agreement is not to be expected and it is important to acknowledge the presence of divergences that reveal the limitations and characteristics inherent to each assay but also to the ligand structure and properties. In this line a number of general considerations should be borne in mind. Firstly, all G4 ligands studied herein are cationic (except NMM) which imply strong electrostatic contribution to their interaction with G4. This is particularly relevant in the FRET-melting assay since, as well-known, electrostatic forces are contributing strongly to stabilization of DNA structures[75] and might explain why the heavily charged ligands (*e.g.* TMPyp4, (4^+)) appear highly efficient whereas their K_D is moderate ("false positive" *e.g.* TMPyP4–/HIV-PRO1, Figure 3 vs Figure 5 and Table 1). As well the binding mode of ligands is a strong determinant of the response in FRET-melting and G4-FID. Globally, PhenDC3, PDC, PDS, BRACO19, RHPS4, Cu-ttpy provide π-stacking on external G4 quartets in a predominant manner, although intercalation may occur in specific conditions and/or with specific sequences.[76-79] Ligands adopting binding mode deviant from external stacking (loop or groove binding) will appear less efficient in FRET-melting (*e.g.* false negative) since binding in DNA grooves has less stabilizing effect than aromatic π-stacking on bases. This holds true also for the G4-FID assay, the formation of a ternary complex should be considered to interpret the poor performances of certain ligands (CX5461, c-PDS) which might result from location in the grooves or redistribution on the second external quartet free for binding. Finally some ligands might have mixed binding modes which may induce ligand distribution to secondary sites if the external quartets are sterically hindered by loops (case of 21CTA, 25CEBwt) or base pairing (HIV-PRO1). As well the occurrence of steric clashes is probable between loops and ligands with dynamic side chains (BRACO19, PDS, c-PDS, Quarfloxin). Hence although 1:1 binding is favored by the stringent conditions applied, species with diverse stoichiometries can be present in solution and vary from one method to another and with regard to the G4/ligand pair partners too. Consequently, the apparent binding affinities sensed by each method can be divergent to some extent. Finally worth mentioning is that FRET-melting may be affected by direct interactions between the ligands and the FRET fluorophores which may modulate the apparent stabilization effect.

Nonetheless, the approach conducted herein using three methods in parallel enable profiling of G4-interactive compounds with high confidence. To come back to the initial goal of our study, the SPR data demonstrate that the combination of FRET-melting and G4-FID can be sufficient for a reliable estimation of the affinity constant of new ligands to the condition that a benchmark compound with a well-characterized binding mode and known K_D is used for calibration. Consequently, we propose to use PhenDC3 as a calibration probe for G4-FID and FRET-melting, whilst applying rigorously the conditions defined for these two assays. The choice of PhenDC3 is based on the outstanding G4 recognition properties of this ligand: K_D in the nanomolar range with all G4 studied, predominant G-

quartet binding mode, poor to no discrimination between G4s. Altogether this makes PhenDC3 a universal G4 probe that, in addition, is commercially available. In establishing as reference the typical profile of PhenDC3 *i.e.* high $\Delta T_{1/2}$ and high % of TO-PRO3 displacement, the comparison with these data could allow to evaluate rapidly the K_D of a new G4 interactive compound. To this end the relative indicator $\Delta\Delta T_{1/2}$ could be used which corresponds to the difference between the $\Delta T_{1/2}$ induced by PhenDC3 and that induced by the ligand to be evaluated ($\Delta\Delta T_{1/2}$ = $\Delta T_{1/2}$ PhenDC3 - $\Delta T_{1/2}$ of studied ligand). Indeed, as shown in Table S7 $\Delta\Delta T_{1/2}$ values falling in the range between 0 and 10 °C defines strong binders. Hence low $\Delta\Delta T_{1/2}$ (between 0 and 5 °C) coupled with a TO-PRO3D > 0.85 will define a strong to high binding behavior with pK_D between 7 to 9; $\Delta\Delta T_{1/2}$ between 5 and 10 °C coupled with 0.6 < TO-PRO3D < 0.85 will define ligand with pK_D 6.5-7. Additionally, using a second probe like BRACO19 that displays properties similar to PhenDC3 (binds all G4s, π-stacking on quartet, commercially available) but with a lower affinity (2 pK_D units) may allow to refine the K_D range. Finally, systematic calibration will also enable to rapidly identify deviant profiles and most interestingly help to discriminate between unusual responses due to methodological bias or ligand aggregation and those with structural significance (highly dynamic loops, steric clashes, groove binding, particular G4 conformation *e.g.* HIV-PRO1 or presence of unfolded forms).

Advantages and shortcomings of each method used in this paper are summarized in Table. 2.

Parameter	**FRET-melting**	**G4-FID**	**SPR**
Signal	Fluorescence (T_m)	Fluorescence (quenching)	Optic (Plasmon)
Data analysis	T_m determination	TO-PRO3 displacement	Resonance angle displacement vs time
Information	Qualitative/Quantitative	Qualitative	Quantitative (Stoichiometry, K_D, binding mode, k_{off} and k_{on})
Temperature	Variable: 25-95°C	Isothermal	Isothermal
System	At Equilibrium	Not at equilibrium	Equilibrium status varies
Number of partners	2 FG4T, G4 ligand	3 G4, probe, G4 ligand	2 G4-biot, G4 ligand
Throughput	High	High	Low
Ionic strength	Near-physiological	Near-physiological	Near-physiological
Volume	Low	Low	low
Main Advantages	Small amount of sample (µM)	Simplicity Small amount of sample (µM)	Small amount of sample High sensitivity

			Quantitative data
Main Limitations / Artefacts	Requires doubly-labelled oligos Interaction with the fluorophores	Compatibility of the probe with the photophysical properties of the G4 ligands Similar binding mode between the probe and the G4 ligand	Surface immobilization High cost

Table 2: Comparison of FRET-melting, G4-FID and SPR to validate G4 binding compounds.

Conclusion

Our study is based on the systematic comparison of the most popular G4 ligands through the use of three biophysical methods in the aim to provide a reliable ranking and guidelines when a ligand has to be chosen for use as G4 probe or G4 drug in biological investigations. On purpose it was decided to focus the study on the comparison of G4-binding affinity since all ligands studied herein have demonstrated high selectivity vs double stranded DNA (> 100 for most) with the exception of TMPyP4. The obtained data were mostly consensus; however, each method has pitfalls and failed to capture the binding properties of all ligands, strongly suggesting the importance of using and comparing different methods to asses G4 ligand binding capacity. The collected data demonstrates that considerable differences exist in the binding strength of the panel of selected compounds. Indeed differences in K_D values up to 5.5 order of magnitude were evidenced. This should inevitably impact the capacity of ligands for reaching their G4 targets in complex biological media implying that important variations are to be expected in their responses supposed to be G4-mediated. Although ligands with moderate affinity can be reliably used in simple biophysical or biochemical systems by simply increasing concentration, weak affinity is more problematic for conducting investigations in complex biological environments (cell extracts, live cells, genome-wide analysis). In those cases, the choice of a high affinity ligand is a prerequisite for proper interpretation of data. Although G4-target recognition can be significantly impacted by cellular barriers and subcellular distribution making that *in vitro* vs *in vivo* performances are not necessarily fully consistent, high target-binding affinity remains nonetheless the mainstay of the pharmacological response of any active principle.[80] Finally the considerable difference between G4 ligands evidenced herein may have crucial consequences when G4 ligands are used for capturing G4 structures in genomes or transcriptomes using pull down technology (G4 Chem-seq etc.). The necessary stringent conditions that warrant specific trapping and isolation of ligand bound to G4-containing fragments, absolutely require strong interactions close or similar to what is observed with antibodies (ChIP-seq).

In conclusion the approach we proposed herein based on the use of PhenDC3 for systematic benchmarking the semi-quantitative assays of FRET-melting and G4-FID represents a simple and rapid way to evaluate the affinity of newly developed G4 ligands before using them to interrogate G4 biology. This should restrict or avoid over-interpretation of the results obtained when exploring the biological consequences of G4-DNA structures, their genomic loci and their potential as therapeutic targets for treatment of diseases.

Supporting information

All experimental procedures and data that support the findings of this study are available in the supplementary material of this article. The authors have cited additional references within the Supporting Information.[7, 52-53, 58-61, 65, 81]

Acknowledgments

This work was supported by CNRS, Université Grenoble Alpes, the French ANR (ANR G4-TopiPro ANR-16-CE11-0006-01), Labex ARCANE and CBH-EUR-GS (ANR-17-EURE-0003) and EIPHI Graduate school (contract "ANR-17-EURE-0002"), the région Auvergne-Rhône-Alpes. EL was funded by the French ANR (ANR Dementia, ANR-17-017-0010, post-doctoral fellowship). The authors acknowledge support from ICMG UAR 2607 for providing synthesis and purification of oligonucleotides and SPR facilities and by the French RENATECH network and its FEMTO-ST technological facility. The authors thank Maéva Morel, Marine Perenon and Marina Pons (SPR experiments) and Joël Lefebvre (preliminary FRET /FID studies).

Conflict of Interests

The authors declare no conflict of interest.

References

[1] K. D. Makova, M. H. Weissensteiner, *Trends Genet.* **2023**, *39*, 109-124.
[2] A. Bacolla, R. D. Wells, *Mol. Carcinog.* **2009**, *48*, 273-285.
[3] J. Choi, T. Majima, *Chem. Soc. Rev.* **2011**, *40*, 5893-5909.
[4] H. J. Lipps, D. Rhodes, *Trends Cell Biol.* **2009**, *19*, 414-422.
[5] M. Tarsounas, M. Tijsterman, *J. Mol. Biol.* **2013**, *425*, 4782-4789.
[6] J. Robinson, F. Raguseo, S. P. Nuccio, D. Liano, M. Di Antonio, *Nucleic Acids Res.* **2021**, *49*, 8419-8431.
[7] A. Piazza, M. Adrian, F. Samazan, B. Heddi, F. Hamon, A. Serero, J. Lopes, M.-P. Teulade-Fichou, A. T. Phan, A. Nicolas, *EMBO J.* **2015**, *34*, 1718-1734.
[8] O. Mendoza, N. M. Gueddouda, J.-B. Boulé, A. Bourdoncle, J.-L. Mergny, *Nucleic Acids Res.* **2015**, *43*, e71-e71.
[9] P. Prorok, M. Artufel, A. Aze, P. Coulombe, I. Peiffer, L. Lacroix, A. Guédin, J.-L. Mergny, J. Damaschke, A. Schepers, C. Cayrou, M.-P. Teulade-Fichou, B. Ballester, M. Méchali, *Nat. Commun.* **2019**, *10*, 3274.
[10] D. Varshney, J. Spiegel, K. Zyner, D. Tannahill, S. Balasubramanian, *Nat. Rev. Mol. Cell Biol.* **2020**, *21*, 459-474.
[11] K. Lyu, E. Y.-C. Chow, X. Mou, T.-F. Chan, Chun K. Kwok, *Nucleic Acids Res.* **2021**, *49*, 5426-5450.
[12] L. Dumas, P. Herviou, E. Dassi, A. Cammas, S. Millevoi, *Trends Biochem. Sci* **2021**, *46*, 270-283.
[13] A. Datta, K. J. Pollock, K. A. Kormuth, R. M. Brosh Jr, *Cytogenet. Genome Res.* **2021**, *161*, 285-296.
[14] G. Biffi, D. Tannahill, J. McCafferty, S. Balasubramanian, *Nat. Chem.* **2013**, *5*, 182.
[15] S. Ray, D. Tillo, R. E. Boer, N. Assad, M. Barshai, G. Wu, Y. Orenstein, D. Yang, J. S. Schneekloth, C. Vinson, *ACS Chem. Biol.* **2020**, *15*, 925-935.
[16] T. Masson, C. Landras Guetta, E. Laigre, A. Cucchiarini, P. Duchambon, M.-P. Teulade-Fichou, D. Verga, *Nucleic Acids Res.* **2021**, *49*, 12644-12660.
[17] A. Piazza, J.-B. Boulé, J. Lopes, K. Mingo, E. Largy, M.-P. Teulade-Fichou, A. Nicolas, *Nucleic Acids Res.* **2010**, *38*, 4337-4348.

[18] S. K. Bharti, J. A. Sommers, F. George, J. Kuper, F. Hamon, K. Shin-ya, M.-P. Teulade-Fichou, C. Kisker, R. M. Brosh, Jr., *J. Biol. Chem.* **2013**, *288*, 28217-28229.
[19] K. G. Zyner, D. S. Mulhearn, S. Adhikari, S. Martínez Cuesta, M. Di Antonio, N. Erard, G. J. Hannon, D. Tannahill, S. Balasubramanian, *eLife* **2019**, *8*, e46793.
[20] J. Spiegel, S. Adhikari, S. Balasubramanian, *Trends Chem.* **2020**, *2*, 123-136.
[21] A. Saha, P. Duchambon, V. Masson, D. Loew, S. Bombard, M.-P. Teulade-Fichou, *Biochemistry* **2020**, *59*, 1261-1272.
[22] O. Reznichenko, A. Quillévéré, R. P. Martins, N. Loaëc, H. Kang, M. J. Lista, C. Beauvineau, J. González-García, R. Guillot, C. Voisset, C. Daskalogianni, R. Fåhraeus, M.-P. Teulade-Fichou, M. Blondel, A. Granzhan, *Eur. J. Med. Chem.* **2019**, *178*, 13-29.
[23] G. Angrand, A. Quillévéré, N. Loaëc, V.-T. Dinh, R. Le Sénéchal, R. Chennoufi, P. Duchambon, M. Keruzoré, Rodrigo P. Martins, M.-P. Teulade-Fichou, R. Fåhraeus, M. Blondel, *Nucleic Acids Res.* **2022**, *50*, 11799-11819.
[24] R. Rodriguez, K. M. Miller, J. V. Forment, C. R. Bradshaw, M. Nikan, S. Britton, T. Oelschlaegel, B. Xhemalce, S. Balasubramanian, S. P. Jackson, *Nat. Chem. Biol.* **2012**, *8*, 301-310.
[25] D. Verga, F. Hamon, F. Poyer, S. Bombard, M.-P. Teulade-Fichou, *Angew. Chem. Int. Ed.* **2014**, *53*, 994-998.
[26] S. Y. Yang, P. Lejault, S. Chevrier, R. Boidot, A. G. Robertson, J. M. Y. Wong, D. Monchaud, *Nat. Commun.* **2018**, *9*, 4730.
[27] I. Renard, M. Grandmougin, A. Roux, S. Y. Yang, P. Lejault, M. Pirrotta, J. M. Y. Wong, D. Monchaud, *Nucleic Acids Res.* **2019**, *47*, 5502-5510.
[28] R. Hänsel-Hertsch, D. Beraldi, S. V. Lensing, G. Marsico, K. Zyner, A. Parry, M. Di Antonio, J. Pike, H. Kimura, M. Narita, D. Tannahill, S. Balasubramanian, *Nat. Genet.* **2016**, *48*, 1267.
[29] S. Neidle, *Nature Reviews Chemistry* **2017**, *1*, 0041.
[30] R. Chaudhuri, S. Bhattacharya, J. Dash, S. Bhattacharya, *J. Med. Chem.* **2021**, *64*, 42-70.
[31] S. Lago, M. Nadai, F. M. Cernilogar, M. Kazerani, H. Domíniguez Moreno, G. Schotta, S. N. Richter, *Nat. Commun.* **2021**, *12*, 3885.
[32] M. Lavigne, O. Helynck, P. Rigolet, R. Boudria-Souilah, M. Nowakowski, B. Baron, S. Brülé, S. Hoos, B. Raynal, L. Guittat, C. Beauvineau, S. Petres, A. Granzhan, J. Guillon, G. Pratviel, M.-P. Teulade-Fichou, P. England, J.-L. Mergny, H. Munier-Lehmann, *Nucleic Acids Res.* **2021**, *49*, 7695-7712.
[33] M. J. Lista, R. P. Martins, O. Billant, M.-A. Contesse, S. Findakly, P. Pochard, C. Daskalogianni, C. Beauvineau, C. Guetta, C. Jamin, M.-P. Teulade-Fichou, R. Fåhraeus, C. Voisset, M. Blondel, *Nat. Commun.* **2017**, *8*, 16043.
[34] S. N. Georgiades, N. H. Abd Karim, K. Suntharalingam, R. Vilar, *Angew. Chem. Int. Ed.* **2010**, *49*, 4020-4034.
[37] J. Zimmer, E. M. C. Tacconi, C. Folio, S. Badie, M. Porru, K. Klare, M. Tumiati, E. Markkanen, S. Halder, A. Ryan, S. P. Jackson, K. Ramadan, S. G. Kuznetsov, A. Biroccio, J. E. Sale, M. Tarsounas, *Mol. Cell* **2016**, *61*, 449-460.
[38] J. Lopes, A. Piazza, R. Bermejo, B. Kriegsman, A. Colosio, M. P. Teulade-Fichou, M. Foiani, A. Nicolas, *EMBO J.* **2011**, *30*, 4033-4046.
[39] K. G. Zyner, A. Simeone, S. M. Flynn, C. Doyle, G. Marsico, S. Adhikari, G. Portella, D. Tannahill, S. Balasubramanian, *Nat. Commun.* **2022**, *13*, 142.
[40] A. De Rache, J.-L. Mergny, *Biochimie* **2015**, *115*, 194-202.
[41] E. Largy, F. Hamon, M.-P. Teulade-Fichou, *Anal. Bioanal. Chem.* **2011**, *400*, 3419-3427.
[44] M. J. Lecours, A. Marchand, A. Anwar, C. Guetta, W. S. Hopkins, V. Gabelica, *Biochim. Biophys. Acta - Gen. Subj* **2017**, *1861*, 1353-1361.
[45] T. Santos, G. F. Salgado, E. J. Cabrita, C. Cruz, *Pharmaceuticals* **2021**, *14*, 769.
[46] S. Neidle, *J. Med. Chem.* **2016**, *59*, 5987-6011.
[47] J.-L. Mergny, L. Lacroix, *Oligonucleotides* **2003**, *13*, 515-537.
[48] P. Thordarson, *Chem. Soc. Rev.* **2011**, *40*, 1305-1323.
[49] M. Read, R. J. Harrison, B. Romagnoli, F. A. Tanious, S. H. Gowan, A. P. Reszka, W. D. Wilson, L. R. Kelland, S. Neidle, *Proc. Natl. Acad. Sci. U.S.A.* **2001**, *98*, 4844-4849.

[50] A. Rizzo, S. Iachettini, P. Zizza, C. Cingolani, M. Porru, S. Artuso, M. Stevens, M. Hummersone, A. Biroccio, E. Salvati, C. Leonetti, *J. Exp. Clin. Cancer Res.* **2014**, *33*, 81.
[51] M. Bončina, Č. Podlipnik, I. Piantanida, J. Eilmes, M.-P. Teulade-Fichou, G. Vesnaver, J. Lah, *Nucleic Acids Res.* **2015**, *43*, 10376-10386.
[52] M. Perenon, H. Bonnet, T. Lavergne, J. Dejeu, E. Defrancq, *PCCP* **2020**, *22*, 4158-4164.
[53] L. Bonnat, L. Bar, B. Génnaro, H. Bonnet, O. Jarjayes, F. Thomas, J. Dejeu, E. Defrancq, T. Lavergne, *Chem. – Eur. J.* **2017**, *23*, 5602-5613.
[54] E. W. White, F. Tanious, M. A. Ismail, A. P. Reszka, S. Neidle, D. W. Boykin, W. D. Wilson, *Biophys. Chem.* **2007**, *126*, 140-153.
[55] D. Drygin, A. Siddiqui-Jain, S. O'Brien, M. Schwaebe, A. Lin, J. Bliesath, C. B. Ho, C. Proffitt, K. Trent, J. P. Whitten, J. K. C. Lim, D. Von Hoff, K. Anderes, W. G. Rice, *Cancer Res.* **2009**, *69*, 7653-7661.
[56] H. Xu, M. Di Antonio, S. McKinney, V. Mathew, B. Ho, N. J. O'Neil, N. D. Santos, J. Silvester, V. Wei, J. Garcia, F. Kabeer, D. Lai, P. Soriano, J. Banáth, D. S. Chiu, D. Yap, D. D. Le, F. B. Ye, A. Zhang, K. Thu, J. Soong, S.-c. Lin, A. H. C. Tsai, T. Osako, T. Algara, D. N. Saunders, J. Wong, J. Xian, M. B. Bally, J. D. Brenton, G. W. Brown, S. P. Shah, D. Cescon, T. W. Mak, C. Caldas, P. C. Stirling, P. Hieter, S. Balasubramanian, S. Aparicio, *Nat. Commun.* **2017**, *8*, 14432.
[57] M. Di Antonio, G. Biffi, A. Mariani, E.-A. Raiber, R. Rodriguez, S. Balasubramanian, *Angew. Chem. Int. Ed.* **2012**, *51*, 11073-11078.
[58] D. Renčiuk, I. Kejnovská, P. Školáková, K. Bednářová, J. Motlová, M. Vorlíčková, *Nucleic Acids Res.* **2014**, *43*, 1985-1985.
[59] K. W. Lim, P. Alberti, A. Guédin, L. Lacroix, J.-F. Riou, N. J. Royle, J.-L. Mergny, A. T. Phan, *Nucleic Acids Res.* **2009**, *37*, 6239-6248.
[60] S. Amrane, M. Adrian, B. Heddi, A. Serero, A. Nicolas, J.-L. Mergny, A. T. Phan, *J. Am. Chem. Soc.* **2012**, *134*, 5807-5816.
[61] S. Amrane, A. Kerkour, A. Bedrat, B. Vialet, M.-L. Andreola, J.-L. Mergny, *J. Am. Chem. Soc.* **2014**, *136*, 5249-5252.
[62] A. De Cian, E. DeLemos, J.-L. Mergny, M.-P. Teulade-Fichou, D. Monchaud, *J. Am. Chem. Soc.* **2007**, *129*, 1856-1857.
[63] T. Lemarteleur, D. Gomez, R. Paterski, E. Mandine, P. Mailliet, J.-F. Riou, *Biochem. Biophys. Res. Commun.* **2004**, *323*, 802-808.
[64] H. Bertrand, D. Monchaud, A. De Cian, R. Guillot, J.-L. Mergny, M.-P. Teulade-Fichou, *Org. Biomol. Chem.* **2007**, *5*, 2555-2559.
[65] R. Bonnet, T. Lavergne, B. Gennaro, N. Spinelli, E. Defrancq, *Chem. Commun.* **2015**, *51*, 4850-4853.
[66] A. Pagano, N. Iaccarino, M. A. S. Abdelhamid, D. Brancaccio, E. U. Garzarella, A. Di Porzio, E. Novellino, Z. A. E. Waller, B. Pagano, J. Amato, A. Randazzo, *Front. chem.* **2018**, *6*.
[67] E. Prado, L. Bonnat, H. Bonnet, T. Lavergne, A. Van der Heyden, G. Pratviel, J. Dejeu, E. Defrancq, *Langmuir* **2018**, *34*, 13057-13064.
[68] G. Piraux, L. Bar, M. Abraham, T. Lavergne, H. Jamet, J. Dejeu, L. Marcélis, E. Defrancq, B. Elias, *Chem. – Eur. J.* **2017**, *23*, 11872-11880.
[69] L. Lecarme, E. Prado, A. De Rache, M.-L. Nicolau-Travers, G. Gellon, J. Dejeu, T. Lavergne, H. Jamet, D. Gomez, J.-L. Mergny, E. Defrancq, O. Jarjayes, F. Thomas, *ChemMedChem* **2016**, *11*, 1133-1136.
[70] J. Dejeu, H. Bonnet, N. Spinelli, E. Defrancq, L. Coche-Guérente, A. Van der Heyden, P. Labbé, *J. Phys. Chem. C* **2018**, *122*, 21521-21530.
[71] T. M. Davis, W. D. Wilson, *Anal. Biochem.* **2000**, *284*, 348-353.
[72] N. C. Sabharwal, V. Savikhin, J. R. Turek-Herman, J. M. Nicoludis, V. A. Szalai, L. A. Yatsunyk, *FEBS J.* **2014**, *281*, 1726-1737.
[73] J. M. Nicoludis, S. P. Barrett, J.-L. Mergny, L. A. Yatsunyk, *Nucleic Acids Res.* **2012**, *40*, 5432-5447.
[74] A. Marchand, D. Strzelecka, V. Gabelica, *Chem. – Eur. J.* **2016**, *22*, 9551-9555.
[75] S. Wang, A. Kumar, K. Aston, B. Nguyen, J. K. Bashkin, D. W. Boykin, W. D. Wilson, *Chem. Commun.* **2013**, *49*, 8543-8545.

[76] W. J. Chung, B. Heddi, F. Hamon, M. P. Teulade-Fichou, A. T. Phan, *Angew. Chem. Int. Ed.* **2014**, *53*, 999-1002.
[77] L.-Y. Liu, T.-Z. Ma, Y.-L. Zeng, W. Liu, Z.-W. Mao, *J. Am. Chem. Soc.* **2022**, *144*, 11878-11887.
[78] A. Kotar, V. Kocman, J. Plavec, *Chem. – Eur. J.* **2020**, *26*, 814-817.
[79] A. Ghosh, M. Trajkovski, M.-P. Teulade-Fichou, V. Gabelica, J. Plavec, *Angew. Chem. Int. Ed.* **2022**, *61*, e202207384.
[80] M. M. Hann, G. L. Simpson, *Methods* **2014**, *68*, 283-285.
[81] P. Murat, R. Bonnet, A. Van der Heyden, N. Spinelli, P. Labbé, D. Monchaud, M.-P. Teulade-Fichou, P. Dumy, E. Defrancq, *Chem. – Eur. J.* **2010**, *16*, 6106-6114.

Uncategorized References

[35] A. Granzhan, R. P. Martins, R. Fåhraeus, M. Blondel, M.-P. Teulade-Fichou, in *Annu. Rep. Med. Chem., Vol. 54* (Ed.: S. Neidle), Academic Press, **2020**, pp. 243-286.
[36] D. Verga, A. Granzhan, M.-P. Teulade-Fichou, in *Handbook of Chemical Biology of Nucleic Acids* (Ed.: N. Sugimoto), Springer Nature Singapore, Singapore, **2022**, pp. 1-57.
[42] G. N. Parkinson, G. W. Collie, in *G-Quadruplex Nucleic Acids: Methods and Protocols* (Eds.: D. Yang, C. Lin), Springer New York, New York, NY, **2019**, pp. 131-155.
[43] A. Funke, K. Weisz, in *G-Quadruplex Nucleic Acids: Methods and Protocols* (Eds.: D. Yang, C. Lin), Springer New York, New York, NY, **2019**, pp. 45-61.

Entry for the Table of Contents

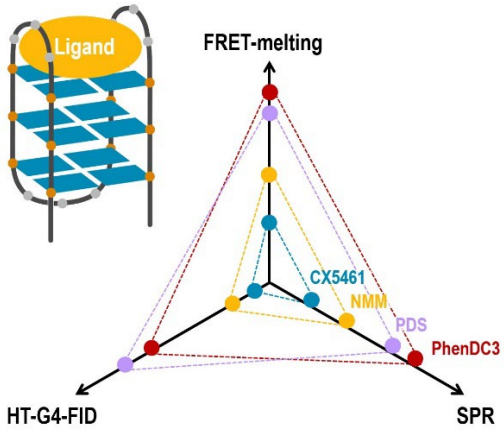

We conducted a systematic affinity ranking of 11 popular G4 ligands vs 5 classical G4 sequences using FRET-melting, G4-FID assays and SPR. This comparative study enables the establishment of a precise affinity ranking of ligands while also highlighting discrepancies attributable to the limitations and characteristics of each assay.